Title

Structure of nanoscale-pitch helical phases: blue phase and twist-bend nematic phase resolved by resonant soft X-ray scattering

Journal

Soft Matter, 13(38)

ISSN

1744-683X

Authors

Salamończyk, Mirosław

Vaupotič, Nataša

Pociecha, Damian

et al.

Publication Date

2017-10-04

DOI

10.1039/c7sm00967d

Peer reviewed

Journal Name

ARTICLE

Structure of nanoscale-pitch helical phases: blue phase and twist-bend nematic phase resolved by resonant soft X-ray scattering

Received 00th January 20xx,
Accepted 00th January 20xx

DOI: 10.1039/x0xx00000x

www.rsc.org/

Mirosław Salamończyk[a,b], Nataša Vaupotič[c,d*], Damian Pociecha[e], Cheng Wang[a], Chenhui Zhu[a*], Ewa Gorecka[e*]

Periodic structures of phases with orientational order of molecules, but homogenous electron density distribution: a short pitch cholesteric, blue phase and twist-bend nematic phase, were probed by a resonant soft x-ray scattering (RSoXS) at the carbon K-edge. The theoretical model shows that in case of a simple heliconical nematic structure two resonant signals corresponding to the full and half pitch band should be present, while only the full pitch band is observed in experiment. This suggests that the twist-bend nematic phase has complex structure with a double-helix, built of two interlocked, shifted helices. We confirm that the helical pitch in the twist-bend nematic phase is in a 10 nm range, for both, the chiral and achiral materials. We also show that the symmetry of a blue phase can unambiguously be determined through a resonant enhancement of the x-ray diffraction signals, by including polarization effects, which are found to be an important indicator in the phase structure determination.

Nanostructured soft materials with hierarchical organization have recently attracted a lot of attention in both fundamental research and applications; the examples of such systems can be found among liquid crystals, gels or structured polymers. The advantage of the chemical diversity of such materials, ranging from low weight molecules to polymers and nanoparticles, is that it enables the intelligent material design by tuning of a particular material functional property, such as electronic or optical energy band gap, polar or magnetic order, etc. Some of these materials may exhibit helical structures or helical morphology; the 'classical' examples of such systems are DNA and peptides, in which helical arrangement of molecules is induced by chirality of molecular building blocks. A variety of helical structures formed by low weight molecules can be found among liquid crystals;[1] chiral mesogenic molecules can self-assemble into a helical nematic or smectic phases, in which molecules uniformly twist, or into a blue phases, a three-dimensional, nanoscale cubic phases formed of double twist cylinders, where each cylinder has an internal, nanoscale helical structure.[1] Less frequent are examples of achiral mesogens (bent-core, dimers, etc.) that exhibit nanoscale helical structures[2]: filaments made either from soft crystal layers[3-5] or smectic membranes,[6] as well as a helioconical nematic phase with an ultra-short, nano-scale helical pitch.[7-14] These materials have recently attracted a lot of attention due to the rich physical phenomena related to the spontaneous symmetry breaking. However, the origin of the helix formation in achiral materials is still on debate, partially due to a limited number of in-situ, experimental probes of orientational order at submicron scale. For some soft matter phases, the orientational order of molecules is coupled to density modulations and, therefore, their structure can be revealed by a standard x-ray diffraction technique, but the phases with a uniform electron density, such as nematic, or blue phases cannot be distinguished by this technique. The method that is sensitive to the spatial variation of the orientation of molecules at nano-scale is a resonant x-ray scattering, which has so far mainly been operated at the absorption edges of Bromine, Selenium and Sulfur for studying the smectic C liquid crystal subphases, to determine their secondary structure induced by the molecular orientation.[15-18] Recently the resonant soft X-ray scattering at the carbon absorption edge has been applied to study a phase separation in block copolymers,[19,20] molecular orientation in solar cells,[21] and morphology of helical nanofilaments (B_4 phase) made of bent-core mesogens.[3]

Here we demonstrate that the RSoXS in combination with theoretical modelling can be used to reveal a 3D structure of phases with a uniform electron density and a periodically modulated orientational order. Furthermore, we show that the polarization analysis is very important in removing the remaining structural degeneracy. We apply the method to blue phases (BP),[22] chiral nematic (N^*) and twist-bend nematic (N_{TB}) phases. The structure of all these phases (Fig. 1) is helical and the twist originates either from the molecular chirality (N^* and BP phases) or is caused by a unique, bent molecular geometry (N_{TB} phase). The N^* phase has a single twisted helical structure, with the average direction of long molecular axes (director)

[a] Advance Light Source, Lawrence Berkeley National Laboratory, Berkeley, CA 94720, USA
[b] Liquid Crystal Institute & Department of Physics, Kent State University, Kent, OH 44242, USA
[c] Department of Physics, Faculty of Natural Sciences and Mathematics, University of Maribor, Koroška 160, 2000 Maribor, Slovenia
[d] Jozef Stefan Institute, Jamova 39, 1000 Lubljana, Slovenia
[e] Faculty of Chemistry, University of Warsaw, Zwirki i Wigury 101, 02-089 Warsaw, Poland

Electronic Supplementary Information (ESI) available: Details of the theoretical model, materials, experimental methods and additional results. See DOI: 10.1039/x0xx00000x

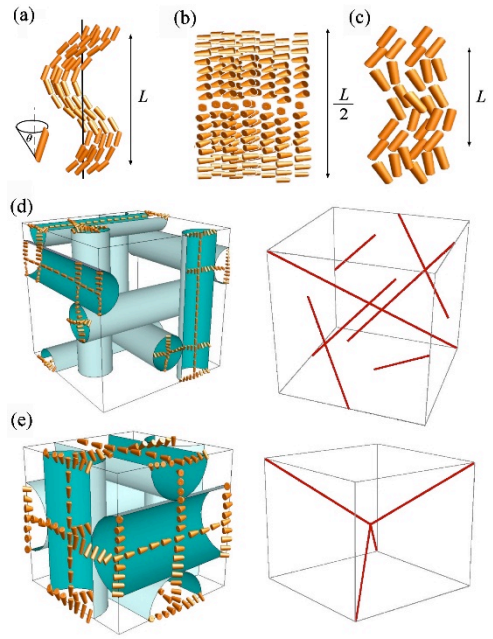

Figure 1. Structure of the (a) twist-bend nematic N_{TB}, (b) chiral nematic N*, (c) splay-bend nematic N_{SB}. *L* is a modulation length. Double twisted cylinders (left) and the defect network (right) in blue phases (d) of type I (BPI) and (e) type II (BPII).

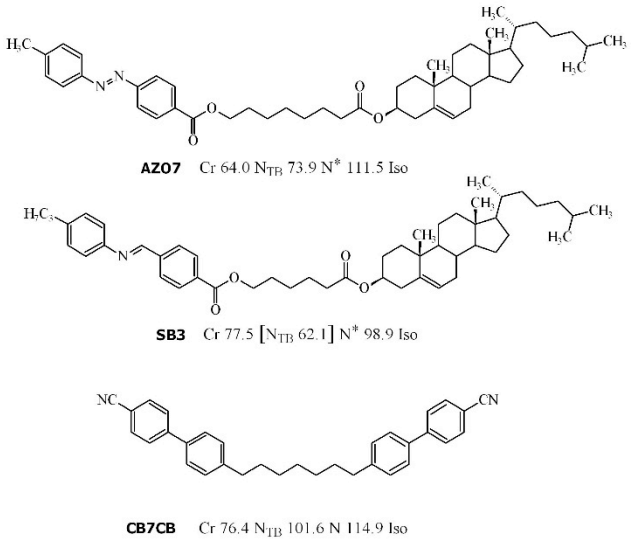

Figure 2. Molecular structure of the studied compounds, **AZO7**, **SB3** and **CB7CB**. For each compound a phase sequence and phase transition temperatures (°C) determined by the differential scanning calorimetry (DSC) on heating scans are given. Note, that for **AZO7** a narrow range of a blue phase between the N* and Iso has been found by microscopic observations; however, it was not recorded on the DSC curves due to a limited resolution. Upon cooling the **AZO7** samples, the blue phase was metastable down to the transition to the N_{TB} phase and thus the cholesteric phase was not observed.

lying in the direction perpendicular to the helix axis. The generally accepted model for the N_{TB} phase is a single, uniform helix with the director processing around the helix axis at some angle θ. For the bent molecules, the non-helical splay-bend nematic (N_{SB}) phase was also predicted,[23,24] in which the modulation of the long molecular axis direction is constrained to the plane; however, so far no clear experimental evidence for the N_{SB} phase was given. In blue phases the twist is induced in every direction perpendicular to the director, resulting in the so called double twist (DT) cylinder. Such DT cylinders cannot continuously fill the space, thus a 3D network of defects is formed with either the body centred (BPI, $I4_132$ symmetry) or simple cubic (BPII, $P4_232$ symmetry) structure. By the elastic x-ray scattering only diffused signals related to the short range positional order are detected in all these phases. For the BP or N^* phases having the helical pitch in the visible or near IR wavelength range, optical methods are used to determine the structure parameters. Here we provide a direct, effective and general approach that can be applied also to structures with periodicities below the optical wavelength, to which neither optical nor classical x-ray diffraction techniques are sensitive to. By RSoXS, the information about the molecular orientational order with the periodicities of the order of a few to hundreds of nanometers can easily be obtained.

We have performed RSoXS measurements for a chiral **SB3**[14] material showing a N^* - N_{TB} phase sequence and a chiral **AZO7**[14,25] compound showing a BP - N_{TB} phase sequence on cooling and N_{TB} - N^* - BP phase sequence on heating (Fig. 2). The results were compared to those obtained for the achiral **CB7CB** dimeric compound, which is a model N_{TB} material showing a N - N_{TB} phase sequence.[8-11,13]

When the chiral material, **AZO7**, is cooled from the isotropic phase, several RSoXS signals are obtained, that can be indexed to the cubic structure (Fig. 3). On further cooling, the signals related to the cubic lattice disappear and a single peak corresponding to a much shorter periodicity appears, signifying a transition to the N_{TB} phase. The position of the signal in the N_{TB} phase is temperature dependent: on cooling the periodicity reduces from 20.3 to 13.3 nm (see SI, Fig. S15). Interestingly, on a subsequent heating, the sample undergoes a transition from the N_{TB} to the N^* phase, in which only one signal corresponding to the half pitch band is observed, at 110 nm (Fig. 3). On further heating, the BP phase is observed only in a narrow temperature range of few degrees, close to the isotropic phase. Apparently, for this material, the BP phase is thermodynamically stable close to the clearing temperature but can easily be supercooled, similarly as observed previously for other dimeric materials.[26]

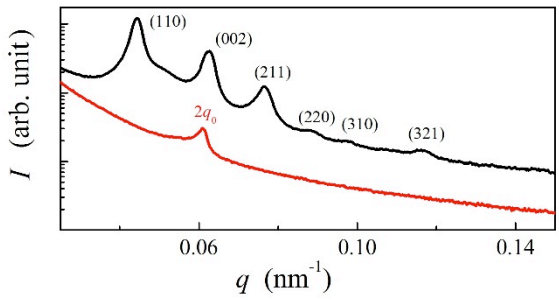

Figure 3. RSoXS patterns, the intensity (*I*) in arbitrary units as a function of the magnitude of the scattering vector *q* for the **AZO7** compound in the BPI (black line) and N^* (red line).

Such a phase sequence enables a direct comparison between the cholesteric pitch and the size of the unit cell of the BP phase. Assuming that the helical pitch at the transition from the cholesteric to the BP phase does not change significantly, the unit cell size in the BPI phase ($I4_132$ symmetry) should correspond to the full pitch length (L) in N* and to the half pitch length ($L/2$) in the BPII phase ($P4_232$ symmetry) (see Fig. 1). Because the first signal in the BP phase of **AZO7** appears at a lower value of q than in the N* phase, the observed blue phase must have the $I4_132$ symmetry (BPI). From the position of the main signals observed in the RSoXS pattern of the cubic phase (peaks (110), (002) and (211)) the crystallographic lattice parameter (a) is obtained: a = 201 nm. Except for the (002) peak the observed peaks are allowed by the symmetry, they are thus resonantly enhanced. A comparison of the position of the purely resonant (002) signal in the BP phase and the half pitch band signal in the N* shows that, within the experimental error, the pitch in the BP phase does not change at the phase transition. In both the BPI and N* phase, the azimuthal position of the signals was strongly sensitive to the polarization of the incoming beam (Fig. 4b,c).

For the **SB3** material, on cooling, the resonant peak corresponding to the half pitch band ($L/2$ ≈ 112 nm) is detected in the N* phase temperature range (Fig. S10). Upon the transition to the N_{TB} phase, the signal corresponding to 11 nm develops. Interestingly, the periodicity detected by the RSoXS experiment in the N_{TB} phase is much smaller than the one measured by the atomic force microscopy (AFM) method, where the fingerprint texture with lines separated by 50-80 nm was observed.[25] The short pitch periodic structure detected by the resonant x-ray method is in line with a large compressibility modulus measured previously.[25] Despite many efforts, the long periodicity detected by the AFM measurements (see SI, Fig. S13), was not observed by the RSoXS method. It is not obvious at the moment, what caused the large periodicity structure detected by the AFM, but one possibility is that the surface free samples, studied by the AFM, have an additional structure induced by chirality, and surfaces cause its destabilization when a thin cell (~ 0.5 μm thick) is used in the x-ray studies reported here. The RSoXS measurements were also repeated for **CB7CB**, the model N_{TB} material.[27] For this compound the resonant peak was also found in the crystal phase: the signal corresponding to the periodicity of 7.8 nm gives the full size of the crystallographic unit cell and corresponds roughly to three molecular distances. Such a signal is forbidden for the $P3_121$ symmetry (the crystal structure was resolved for the **CB9CB** homologue[28]) and is thus not observed in the elastic diffraction experiments. The melting of the crystal and the transition to the N_{TB} phase is associated with a sudden jump of the peak position to 8.2 nm (Fig. 5). This clearly shows that the structures of the crystal and N_{TB} phases are closely related and probably caused by steric interactions[28,29] rather than by the elastic[24] or flexoelectric[23,29,30] effect.

Interestingly, the scattering patterns of N* and BP show strong intensity anisotropy, but that of the N_{TB} does not. To fully understand the resonant x-ray diffraction pattern, one has to calculate the dispersion correction to the structure factor, which is proportional to the Fourier transform of the spatially dependent structure polarizability.[32,33] We have obtained the dispersion correction for the LC phases shown in Fig. 1 and found the scattered intensity as a function of the polarization direction of the incident beam and biaxiality of the x-ray susceptibility.

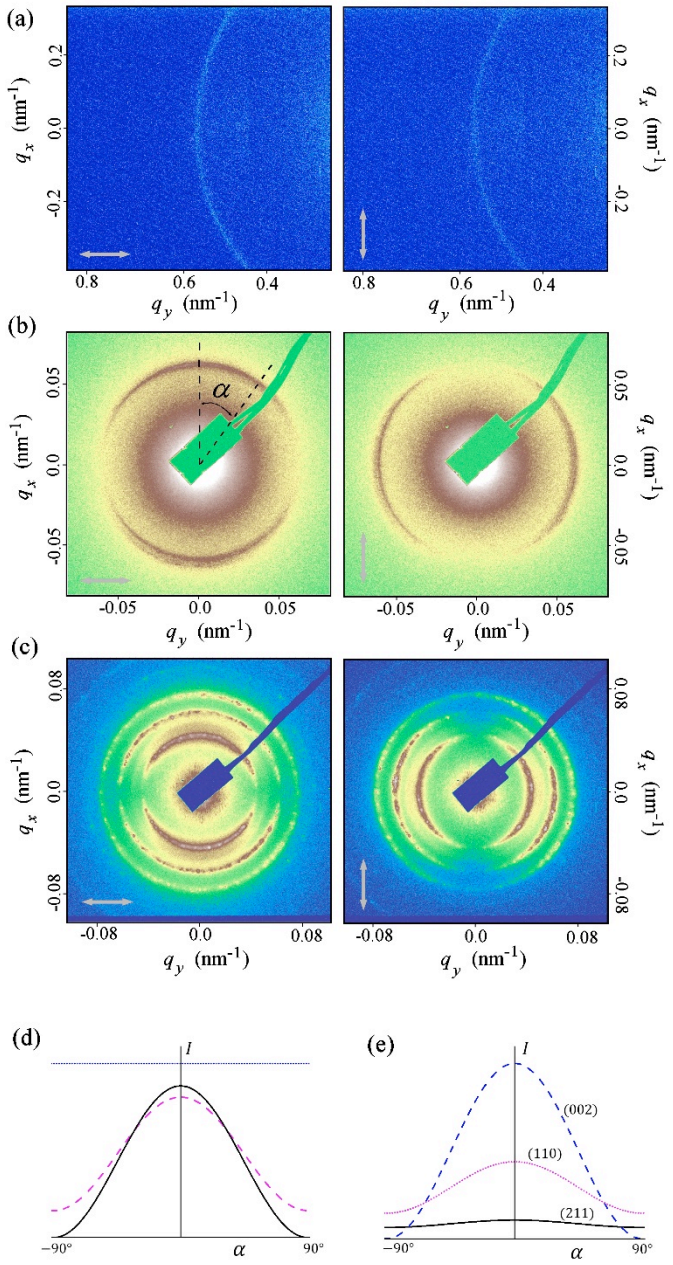

Figure 4. RSoXS patterns of the **SB3** compound in N_{TB} phase (a) and **AZO7** compound in N* (b) and BPI (c) phases recorded for two perpendicular polarizations of the incident beam. d) Theoretically calculated intensity in arbitrary units as a function of the azimuthal angle α; $2q_0$ peak in N* (black solid line); $2q_0$ (magenta dashed line) and q_0 (blue dotted line) peak in N_{TB}, both calculated at the cone angle θ =10 deg. To present the results on the same graph, the intensity of the N* peak was divided by 10 and the intensity of the $2q_0$ peak in N_{TB} was multiplied by 100. (e) The intensities of the three most intensive peaks in the BPI phase. Parameter values: f_1/f_2 = 0.6, where f_1, f_2 and -(f_1+f_2) are the eigenvalues of the local traceless dispersion correction to the form factor (see SI).

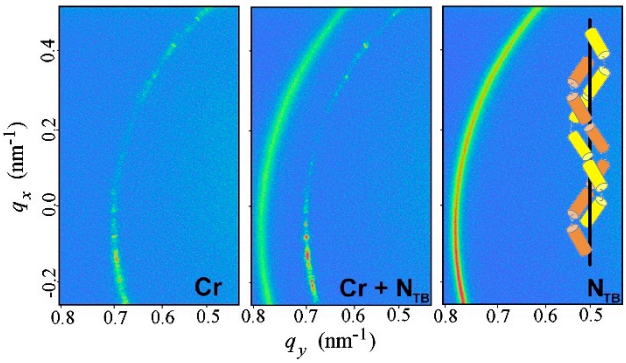

Figure 5. Two dimensional RSoXS patterns for the **CB7CB** compound in the crystalline (Cr) and twist-bend nematic phase (N_{TB}) and in the temperature range of the phase coexistence. The observed signals correspond to the periodicities of 7.8 nm in Cr and 8.2 nm in N_{TB}. In the inset – a simplified model of N_{TB} phase structure with two interlocked, mutually shifted helices.

Details of calculations are given in the Supplementary Information (SI), here we give only the main results. In the N^* phase only the half pitch peak at $2q_0$ is expected, where $q_0=2\pi/L$ is the magnitude of the wave vector of the helical structure and L is the helical pitch. In N^* the $2q_0$ signal intensity is very sensitive to the polarization of the incident x-ray beam, as expected, because the beam with the electric field polarized perpendicular to the helix detects the highest contrast in the director modulation, while the beam polarized along the helix axis detects the uniform structure of the short molecular axes. As a result, for a powder sample, in which the helix axis directions are randomly distributed in space, a 2D scattering pattern exhibits anisotropy for the linearly polarized incident x-ray beam. Two complementary parts of the diffraction ring are predicted in the diffraction pattern, if the polarization of the incident beam is rotated by 90 deg. For the N_{TB} and N_{SB} phases the model predicts two signals, at q_0 and $2q_0$. Interestingly, the q_0 and $2q_0$ signals have a different sensitivity to the polarization of the x-ray beam; the q_0 signal is invariant to the polarization direction while for the $2q_0$ signal in the N_{TB} phase the dependence is similar to the one observed in the N^* phase (SI, Fig. S3). Experimentally, only one peak has been found in the N_{TB} phase, which shows no intensity anisotropy, suggesting that the peak is the q_0 signal, corresponding to a 360 deg rotation of molecular director around the helical axis. It should be pointed out that for none of the N_{TB} materials studied so far the signal corresponding to a half pitch band ($2q_0$) was detected. Previous RSoXS experiments at the carbon K-edge on **CB7CB**[27] as well as measurements performed using the x-ray scattering at the Selenium K-edge,[34] also give a systematic lack of the $2q_0$ signal in the N_{TB} phase. Analysing the reasons for the lack of the $2q_0$ signal let us first point out that the intensity of the $2q_0$ peak can be much lower than the intensity of the q_0 peak, as shown by the theoretical calculations in SI. The ratio of the intensities of these two peaks depends on the ratio of the eigenvalues of the anisotropic part of the molecular polarizability. If this ratio is close to 1, the intensity of the $2q_0$ peak can be negligibly small (see Fig. S4b in SI). However, based on the measurements performed in the blue phase of one of the materials exhibiting also the N_{TB} phase (Azo7), the ratio between the eigenvalues seems to be significantly different from 1 and in this material, the intensity of the $2q_0$ peak in the N_{TB} phase should be comparable to the intensity of the q_0 peak. Other possible reasons for the suppression of the $2q_0$ peak are thermal fluctuations (the Debye-Waller effect), self-absorption and a finite correlation length for helical modulations. If we assume, that the amplitude of the thermally induced displacement of the helical pitch is lower than 10% of the pitch length, the decrease in intensity of the $2q_0$ peak compared to the q_0 peak would not be more than approximately 30%. The self-absorption in a thin cell and at this angle range would reduce the signal intensity proportionally to the increased optical path length, i. e. by few %. The effect of the limited correlation length can be excluded as the width of the q_o signal is comparable to the machine resolution, denoting a long-range order. Because of the systematic lack of the $2q_0$ peak in all the materials studied so far[34,27], we thus propose a more fundamental reason for the absence of the $2q_0$ signal. We suggest that the structure is actually made of two interlocked helices, which are mutually shifted (Fig. 5). The calculations show that the $2q_0$ peak is cancelled out for the shift between helices equal to $L/4$. The shift can be induced by short-range interactions of dimers that favour a local intercalated arrangement of the neighbouring molecules,[29] which seems to be quite common for dimeric molecules.[34] The tendency for the formation of interlocked helices is probably general for bent dimers, as the crystal structure of the **CB9CB** homologue[28] is also formed of interlocked and shifted helices, which are made of two types of slightly different molecular conformers. Very recently, a duplex double-helical molecular chain was proposed as a building motif of NTB phase by the Boulder group.[35]

For the blue phases formed of double twisted cylinders, we calculated the positions of the elastic diffraction peaks by building up the structure from infinitely long cylinders. The Fourier transform of the cubic lattice filled with cylinders of a finite width and uniform density formally gives the (*hkl*) diffraction signals if at least one of the Miller index, *h*, *k* or *l*, is zero (SI, Tab. S1). However, because the cylinders are in contact, the density of the unit cell is practically uniform and none of these peaks is observed in the elastic scattering. If the electron density in the defect regions between the cylinders is different than in cylinders (Fig. 1) the signals allowed by the $P4_232$ (BPII) or $I4_132$ (BPI) symmetry should be detected. In practice, none of these signals is found by the elastic x-ray scattering, confirming that the electron density difference between the cylinders and defect regions is negligible. In order to include the resonant effects, the dispersion correction was calculated due to the helical spatial variation of the director in the direction perpendicular to the cylinder axis and by arranging the cylinders into a proper cubic lattice (Fig. 1). We show that some signals allowed by the symmetry of the BP phases, but not detectable by the elastic x-ray diffraction, become visible in the resonant x-ray diffraction due to their enhancement by orientation modulations (Tab. 1).

Additionally, purely resonant signals: (001) for $P4_232$ and (002) for $I4_132$ are predicted.

In the BPI phase intensities of all the signals are sensitive to the polarization of the incident x-ray beam. For a powder sample, the two most intensive signals, (110) and (002), have the same polarization dependence as the half-pitch band signal in the N^* phase and the complementary parts of the diffraction rings are predicted for the incident beams polarized in perpendicular directions. The polarization dependence of the (211) signal is defined by the biaxiality of the susceptibility. For strongly biaxial molecules, such as bent dimers, the dependence is similar to that observed for the (110) and (002) signals.

Table 1. The resonant or resonantly enhanced diffraction signals in the BPI and BPII phases. Ticks denote the peaks with a non-zero intensity. The (002) peak in the BPI, and the (001) peak in the BPII are purely resonant signals; the other observable signals are resonantly enhanced.

(*hkl*)	(001)	(110)	(111)	(002)	(210)	(211)	(220)
BPII	✓	✓	✓	✓	✓	✓	✓
BPI	x	✓	x	✓	X	✓	✓
(*hkl*)	(221)	(310)	(311)	(222)	(320)	(321)	
BPII	✓	✓	✓	x	✓	✓	
BPI	x	x	x	✓	X	✓	

In the BPI phase intensities of all the signals are sensitive to the polarization of the incident x-ray beam. For a powder sample, the two most intensive signals, (110) and (002), have the same polarization dependence as the half-pitch band signal in the N^* phase and the complementary parts of the diffraction rings are predicted for the incident beams polarized in perpendicular directions. The polarization dependence of the (211) signal is defined by the biaxiality of the susceptibility. For strongly biaxial molecules, such as bent dimers, the dependence is similar to that observed for the (110) and (002) signals.

Conclusions

We have shown that the comparison between the RSoXS signals in blue phases and N^* phase enable a straightforward determination of the type of the blue phase. We have also shown that the modulation pitch in the N_{TB} phase is of the same order of magnitude for both, the chiral and achiral materials. However, the structure of the twist-bend nematic phase seems to be to be more complex than commonly accepted. The theoretical model shows that, in the case of the heliconical structure, RSoXS signals corresponding to the full and half pitch band should both be present and they should have a very different polarization dependence. Experimentally, only one signal was found, with the intensity independent of the beam polarization; it was thus unambiguously identified as the full pitch band. The lack of the half pitch band strongly suggests that the N_{TB} structure is made of two interlocked and shifted helices.

Conflicts of interest

There are no conflicts of interest to declare.

Acknowledgements

MS acknowledges the support of the U.S. National Science Foundation I2CAM International Materials Institute Award, Grant DMR-1411344 and NSF grant DMR-1307674.

NV acknowledges the financial support from the Slovenian Research Agency (research core funding No. P1-0055). EG and DP acknowledge the support of the National Science Centre (Poland) under the grant no. 2016/22/A/ST5/00319.

The authors acknowledge the important technical help and discussions from Drs. A. Kilcoyne, M. Brady, G. Su and A. Hexemer at the ALS LBNL and the synthesis of the studied materials by A. Zep.

The beam line 11.0.1.2 at the Advanced Light Source is supported by the Director of the Office of Science, Office of Basic Energy Sciences, of the U.S. Department of Energy under Contract No. DE-AC02- 05CH11231.

The authors thank the referees for the fruitful discussion through the refereeing process regarding both the theoretical model and interpretation of experimental results.

Notes and references

1 *Chirality in Liquid Crystals*, ed. H. Kitzerow, C. Bahr, Springer-Verlag New York, 2001.

2 C. Tschierske, G. Ungar, *ChemPhysChem,* 2016, **17**, 9 – 26

3 C. Zhu, C. Wang, A. Young, F. Liu, I. Gunkel, D. Chen, D. Walba, J. Maclennan, N. A. Clark, A. Hexemer, *Nano Lett*. 2015, **15**, 3420–3424.

4 L. E. Hough, H. T. Jung, D. Krüerke, M. S. Heberling, M. Nakata, C. D. Jones, D. Chen, D. R. Link, J. Zasadzinski, G. Heppke, J. P. Rabe, W. Stocker, E. Körblova, D. M. Walba, M. A. Glaser, N. A. Clark, *Science,* 2009, **325**, 456-460.

5 J. Matraszek, N. Topnani, N. Vaupotič, H. Takezoe, J. Mieczkowski, D. Pociecha, E. Gorecka, *Angew. Chem. Int. Ed.* 2016, **55**, 3468–3472.

6 L. E. Hough, M. Spannuth, M. Nakata, D. A. Coleman, C. D. Jones, G Dantlgraber, N. A. Clark, *Science,* 2009, **325**, 452-456.

7 G. Pelzl, A. Eremin S. Diele, H. Kresse, W. Weisflog, *J. Mater. Chem*. 2002, **12**, 2591-2593.

8 M. Cestari, S. Diez-Berart, D. A. Dunmur, A. Ferrarini, M. R. de la Fuente, D. J. B. Jackson, D. O. Lopez, G. R. Luckhurst, M. A. Perez-Jubindo, R. M. Richardson, J. Salud, B. A. Timimi, H. Zimmermann, , *Phys. Rev. E* 2011, **84**, 031704.

9 C. Meyer, G. R. Luckhurst, I. Dozov, *Phys. Rev. Lett*. 2013, **111**, 067801.

10 D. Chen, J. H. Porada, J. B. Hooper, A. Klittnick, Y. Shen, M. R. Tuchband, E. Korblova, D. Bedrov, D. M. Walba, M. A. Glaser, J. E. Maclennan, N. A. Clark, *Proc. Natl. Acad. Sci*. 2013, **110**, 15931–15936.

11 V. Borshch, Y.-K. Kim, J. Xiang, M. Gao, A. Jakli, V. P. Panov, J. K. Vij, C. T. Imrie, M. G. Tamba, G. H. Mehl, O. D. Lavrentovich, *Nat. Commun*. 2013, **4**, 1–8.

12 D. Chen, M. Nakata R. Shao, M. R. Tuchband, M. Shuai, U. Baumeister, W. Weissflog, D. M. Walba, M. A. Glaser, J. E. Maclennan, N. A. Clark, *Phys. Rev. E* 2014, **89**, 022506.

13 E. Górecka, M. Salamończyk, A. Zep, D. Pociecha, C. Welch, Z. Ahmed, G. H. Mehl, *Liq. Cryst*. 2015, **42**, 1–7.

14 A. Zep, S. Aya, K. Aihara, K. Ema, D. Pociecha, K. Madrak, P. Bernatowicz, H. Takezoe, E. Gorecka, *J. Mater. Chem. C* 2013, **1**, 46.
15 P. Mach, R. Pindak, A.-M. Levelut, P. Barois, H. Nguyen, C. Huang, L. Furenlid, *Phys. Rev. Lett*. 1998, **81**, 1015–1018.
16 P. Fernandes, P. Barois, S. T. Wang, Z. Q. Liu, B. K. McCoy, C. C. Huang, R. Pindak, W. Caliebe, H. T. Nguyen, *Phys. Rev. Lett*. 2007, **99**, 1–4.
17 C. L. Folcia, J. Ortega, J. Etxebarria, S. Rodríguez-Conde, G. Sanz-Enguita, K. Geese, C. Tschierske, V. Ponsinet, P. Barois, R. Pindak, L.-D. Pan, Z. Q. Liu, B. K. McCoy, C. C. Huang, *Soft Matter* 2014, **10**, 196–205.
18 H. F. Gleeson, L. S. Hirst, *ChemPhysChem,* 2006, **7**, 321–328.
19 C. Wang, D. H. Lee, A. Hexemer, M. I. Kim, W. Zhao, H. Hasegawa, H. Ade, T. P. Russell, *Nano Lett*. 2011, **11**, 3906–3911.
20 J. M. Virgili, Y. F. Tao, J. B. Kortright, N. P. Balsara, R. a. Segalman, *Macromolecules* 2007, **40**, 2092–2099.
21 J. R. Tumbleston, B. a. Collins, L. Yang, A. C. Stuart, E. Gann, W. Ma, W. You, H. Ade, *Nat. Photonics* 2014, **8**, 385–391.
22 D. C. Wright, N. D. Mermin, *Rev. Mod. Phys*. 1989, **61**, 385–432.
23 R. B. Meyer in Structural Problems in Liquid Crystal Physics, ed. Balian R. and Weil G., Les Houches Summer School in Theoretical Physics, 1973. *Molecular Fluids*, Gordon and Breach, New York, 1976, 273–373.
24 I. Dozov, *Europhys. Lett*. 2007, **56**, 247–253.
25 E. Gorecka, N. Vaupotič, A. Zep, D. Pociecha, J. Yoshioka, J. Yamamoto, H. Takezoe, *Angew. Chemie Int. Ed*. 2015, **54**, 10155–10159.
26 H. J. Coles, M. N. Pivnenko, *Nature,* 2005, **436**, 997–1000.
27 C. Zhu, M. R. Tuchband, A. Young, M. Shuai, A. Scarbrough, D. M. Walba, J. E. Maclennan, C. Wang, A. Hexemer, N. A. Clark, *Phys. Rev. Lett*. 2016, **116**, 147803.
28 K. Hori, M. Iimuro, A. Nakao, H. Toriumi, *J. Mol. Struct*. 2004, **699**, 23–29.
29 N. Vaupotič, S. Curk, M. A. Osipov, M. Čepič, H. Takezoe, E. Gorecka, *Phys. Rev. E* 2016, **93**, 22704.
30 S. M. Shamid, S. Dhakal, J. V. Selinger, Phys. Rev. E 2013, **87**, 052503.
31 N. Vaupotič, M. Čepič, M. A. Osipov, E. Gorecka, *Phys. Rev. E,* 2014, **89**, 030501(R).
32 D. H. Templeton, L. K. Templeton, *Acta Crystallogr. Sect. A,* 1980, **36**, 237–241.
33 V. E. Dmitrienko, *Acta Crystallogr. Sect. A,* 1983, **39**, 29–35.
34 W. D. Stevenson, Z. Ahmed, X. B. Zeng, C. Welch, G. Ungar, G. H. Mehl, *arXiv,* 2016, 1612.01180.
35 M. R. Tuchband, M. Shuai, K. A. Graber, D. Chen, C. Zhu, L. Radzihovsky, A. Klittnick, L. M. Foley, A. Scarbrough, J. H. Porada, M. Moran, J. Yelk, D. Bedrov, E. Korblova, D. M. Walba, A. Hexemer, J. E. Maclennan, M. A. Glaser, N. A. Clark, *arXiv*, 2017, 1703.10787

